Standoff Acoustic Shear Wave Imaging Using LFM Chirps

Glenwood Garner and Michael B. Steer
Department of Electrical and Computer Engineering
NC State University
Raleigh, North Carolina, USA, 27606

Abstract: *Shear wave seismic-acoustic imaging incorporating laser Doppler vibrometers (LDV) has been successfully used to detect buried landmines using single tone excitation. In this paper, the use of linear frequency modulated (LFM) chirps is proposed to exploit wideband resonant behavior. This technique captures more information about complex elastic inhomogeneities while being more tolerant to noise.*

Keywords: acoustic imaging; acoustic sensors; landmine detection.

Introduction

Shear wave elasticity imaging (SWEI) is a method of "remote palpation" used to find cancerous inhomogeneities buried deep in healthy tissue[1]-[3]. Similar techniques of measuring surface waves have been used by Xiang and Sabatier to locate shallow buried landmines [4],[5]. In these methods acoustic energy is coupled into the medium in the form of a shear wave, and the response of the medium to the incident energy reveals information about the presence of an inhomogeneity, defined here as a mass contained within the homogeneous region with substationally different stiffness, density, or Poisson's ratio. The change in these material properties locally changes the wave propagation speed and affects the amplitude of standing modes and scattered waves, typically appearing as an area of reduced vibration amplitude.

In contrast to typical SWEI applications, which rely on contacting shakers and Doppler ultrasound to image tumors, this technique strives for standoff detection. The biggest contrast here is the use of low frequency acoustics as the excitation source, which produces plane wave excitation in the far field of the transmitter. The boundary condition used in [1] must be modified to account for plane wave excitation. Furthermore, due to the longitudinal nature of acoustic waves, Gao's model is modified for longitudinal scattering, which is typically ignored due to the large wavelengths in biological tissue. For the test material presented in this paper (expanded polystyrene foam), the shear and longitudinal waves speeds are almost equal allowing the latter to be measured at the surface where mode conversion produces a composite of shear and longitudinal waves. Finally, this paper presents a finite difference time domain (FDTD) approach utilizing LFM chirps as the excitation waveform. This method captures broadband information about resonant modes while being more tolerant to noise at any particular frequency.

Wave Propagation in Inhomogeneous Materials

Consider a linear, isotropic, elastic material that has a longitudinal displacement field vector ξ_l satisfying [6]

$$\nabla^2 \xi_l - \frac{1}{c_l^2}\frac{\partial^2 \xi_l}{\partial t^2} = 0, \tag{1}$$

with propagation velocity of

$$c_l^2 = \frac{E}{2\rho(1+\nu)(1-2\nu)}. \tag{2}$$

Here E is the Young's modulus of elasticity, ρ is the density, and ν is Poisson's ratio. Within the homogeneous region, we insert an elastic 'inhomogeneity' as depicted in Fig. 1. This area has dimensions $L_a' \times L_b'$, and is centered at (x_0,y_0), and has propagation speed significantly different than the surrounding homogeneous region. Both the homogeneous and inhomogeneous regions have displacement field vectors that satisfy (1), but with different propagation speeds. In traditional SWEI, the most distinguishable mechanical property that separates tumor from normal tissue is the stiffness, but here we utilize the change in density and Poisson's ratio as well. Utilizing a piecewise approach, the homogenous longitudinal wave speed is [1]

$$c_0^2(\mathbf{x}) = \begin{cases} \dfrac{E_0}{2\rho_0(1+\nu_0)(1-2\nu_0)} & \text{for } 0 \le x < L_a,\ 0 \le y < L_b \\ 0 & \text{for inhomogeneity} \end{cases} \tag{3}$$

while the inhomogeneous longitudinal wave speed is

$$c_1^2(\mathbf{x}) = \begin{cases} 0 & \text{for } 0 \le x < L_a,\ 0 \le y < L_b \\ \dfrac{E_1}{2\rho_1(1+\nu_1)(1-2\nu_1)} & \text{for inhomogeneity} \end{cases} \tag{4}$$

where $\mathbf{x}$ is the position vector. Utilizing the relation

$$\gamma(\mathbf{x}) = \begin{cases} \left(c_1^2 - c_0^2\right)/c_0^2 & \text{for inhomogeneous area } L_a' L_b' \\ 0 & \text{for homogenous area} \end{cases} \tag{5}$$

the sound speed for the entire region can be defined as [3]

$$c^2 = c_0^2\left(1+\gamma(\mathbf{x})\right). \tag{6}$$

Report Documentation Page

Form Approved
OMB No. 0704-0188

1. REPORT DATE	2. REPORT TYPE	3. DATES COVERED
21 MAR 2011	**Final**	**1 Aug 2010 - 31 Dec 2016**

4. TITLE AND SUBTITLE
Standoff acoustic shear wave imaging using LFM chirps / Conference: GOMAC 2011

5a. CONTRACT NUMBER
N/A

5b. GRANT NUMBER
N00014-10-1-0958

5c. PROGRAM ELEMENT NUMBER
N/A

6. AUTHOR(S)
Glenwood Garner, Michael B. Steer / North Carolina State University

5d. PROJECT NUMBER
N/A

5e. TASK NUMBER
N/A

5f. WORK UNIT NUMBER
N/A

7. PERFORMING ORGANIZATION NAME(S) AND ADDRESS(ES)
North Carolina State University Electrical & Computer Engineering 890 Oval Dr., 3114 Engineering Building II Raleigh, NC 27695

8. PERFORMING ORGANIZATION REPORT NUMBER
36

9. SPONSORING/MONITORING AGENCY NAME(S) AND ADDRESS(ES)
Office of Naval Research (ONR) 875 North Randolph Street - Suite 1425 Code 03R Arlington, VA 22203-1995

10. SPONSOR/MONITOR'S ACRONYM(S)
ONR

11. SPONSOR/MONITOR'S REPORT NUMBER(S)
N/A

12. DISTRIBUTION/AVAILABILITY STATEMENT
Approved for public release, distribution unlimited

13. SUPPLEMENTARY NOTES
Conference Paper, The original document contains color images.

14. ABSTRACT
Shear wave seismic-acoustic imaging incorporating laser Doppler vibrometers (LDV) has been successfully used to detect buried landmines using single tone excitation. In this paper, the use of linear frequency modulated (LFM) chirps is proposed to exploit wideband resonant behavior. This technique captures more information about complex elastic inhomogeneities while being more tolerant to noise.

15. SUBJECT TERMS
acoustic imaging; acoustic sensors; landmine detection

16. SECURITY CLASSIFICATION OF:			17. LIMITATION OF ABSTRACT	18. NUMBER OF PAGES	19a. NAME OF RESPONSIBLE PERSON
a. REPORT	b. ABSTRACT	c. THIS PAGE			
unclassified	**unclassified**	**unclassified**	**SAR**	**4**	

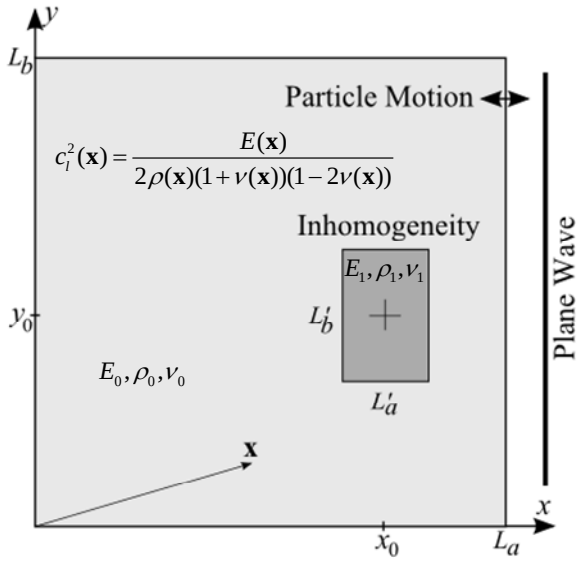

Figure 1. Two dimensional geometry of longitudinal scattering. The size of the homogeneous region is $L_a \times L_b$, with inhomogeneity located at (x_0, y_0) of dimension $L_a' \times L_b'$.

Since acoustic plane waves are longitudinal and the shear and longitudinal wave speeds are approximately equal in our homogenous test case, (1) and (2) will form the basis of our FDTD model. The subscripts '*s*' and '*i*' will now be used to distinguish scattered and incident waves respectively. We will also limit propagation to the *x*-*y* plane, effectively making the target infinite in the *z* axis. With the longitudinal sound speed defined over the entire region, (2a) is now rewritten as [3]

$$\nabla^2 \xi - \frac{1}{c_0^2\left(1+\gamma(\mathbf{x})\right)} \frac{\partial^2 \xi}{\partial t^2} = 0. \tag{7}$$

Loss may be added by including a relaxation term so that (7) becomes [1]

$$\nabla^2 \xi - \frac{1}{c_0^2\left(1+\gamma(\mathbf{x})\right)} \frac{\partial^2 \xi}{\partial t^2} - \frac{R}{\rho c_0^2\left(1+\gamma(\mathbf{x})\right)} \frac{\partial \xi}{\partial t} = 0, \tag{8}$$

where $R = (\omega\rho_0)/Q$, and Q is the quality factor of the material at the excitation frequency ω.

Finite Difference Time Domain Solution

The use of LFM chirps does not allow a finite difference frequency domain solution or analytic solutions to easily be used. A simple approach to solutions of such scattering problems is a finite difference time domain method. To begin with, we split ξ into incident and scattered waves,

$$\xi = \xi_i + \xi_s, \tag{9}$$

where ξ_i is the incident longitudinal wave and ξ_s is the scattered longitudinal wave. Substituting (9) into (8) and applying

$$\nabla^2 \xi_i - \frac{1}{c_0^2} \frac{\partial \xi_i}{\partial t^2} - \frac{R}{\rho_0 c_0^2} \frac{\partial \xi_i}{\partial t} = 0 \tag{10}$$

yields

$$\nabla^2 \xi_s - \frac{1}{c_0^2} \frac{\partial^2 \xi_s}{\partial t^2} - \frac{R}{\rho_0 c_0^2} \frac{\partial \xi_s}{\partial t} = -\frac{1}{c_0^2} \frac{\gamma(\mathbf{x})}{1+\gamma(\mathbf{x})} \frac{\partial^2}{\partial t^2}\left(\xi_i + \xi_s\right) - \frac{R}{\rho_0 c_0^2} \frac{\lambda(\mathbf{x})}{1+\gamma(\mathbf{x})} \frac{\partial}{\partial t}\left(\xi_i + \xi_s\right). \tag{11}$$

Since the amplitude of ξ_s is much smaller than that of ξ_i, we may utilize the Born approximation and discard the ξ_s terms in the right side of (11) resulting in [1]

$$\nabla^2 \xi_s - \frac{1}{c_0^2} \frac{\partial^2 \xi_s}{\partial t^2} - \frac{R}{\rho_0 c_0^2} \frac{\partial \xi_s}{\partial t} = -\frac{1}{c_0^2} \frac{\gamma(\mathbf{x})}{1+\gamma(\mathbf{x})} \frac{\partial^2 \xi_i}{\partial t^2} - \frac{R}{\rho_0 c_0^2} \frac{\lambda(\mathbf{x})}{1+\gamma(\mathbf{x})} \frac{\partial \xi_i}{\partial t} \tag{12}$$

Gao, Parker, and Alam derived a similar equation for shear waves [1]. Using several more simplifying assumptions, they were able to derive a complicated closed form solution. In contrast, this paper presents a simple FDTD solution for LFM chirp excitations at the boundary resulting from plane waves in the farfield of an acoustic source. The finite difference method may be applied to (12) yielding

$$\begin{aligned}
&\xi_s(x, y, t+\Delta t) = \\
&\frac{2\rho_0 c_0^2 \Delta t^2}{2\rho_0 + R\Delta t}\left[\frac{1}{\Delta x^2 \Delta y^2}\left(\xi_s(x-\Delta x, y, t) + \xi_s(x+\Delta x, y, t)\right.\right. \\
&\left. + \xi_s(x, y-\Delta y, t) + \xi_s(x, y+\Delta y, t) - 4\xi_s(x, y, t)\right) \\
&- \xi_s(x, y, t-\Delta t)\left(\frac{1}{c_0^2 \Delta t^2} - \frac{R}{2\rho_0 c_0^2 \Delta t}\right) + \frac{2\xi_s(x, y, t)}{c_0^2 \Delta t^2} \\
&- \frac{\gamma(x)}{1+\gamma(x)}\left[\frac{1}{c_0^2 \Delta t^2}\left(\xi_i(x, y, t-\Delta t) - 2\xi_i(x, y, t)\right.\right. \\
&\left.\left. + \xi_i(x, y, t+\Delta t)\right) + \frac{R}{2\rho_0 c_0^2 \Delta t}\left(\xi_i(x, y, t+\Delta t)\right.\right. \\
&\left.\left. - \xi_i(x, y, t-\Delta t)\right)\right].
\end{aligned} \tag{13}$$

Examination of (12) and (16) reveals that the scattered displacement vector created by an inhomogeneity is dependent upon the incident displacement vector ξ_i, which has non-zero amplitude regardless of whether an inhomogeneity is present. Setting $\gamma(\mathbf{x}) = 0$ in (8) or (12) reduces the wave equation to that describing only the incident wave, (i.e. $\xi_s = 0$). The solution for the incident displacement field vector may be computed by a similar finite difference method yielding

$$\xi_i(x,y,t+\Delta t) = \frac{2\rho_0 c_0^2 \Delta t^2}{2\rho_0 + R\Delta t}\left[\frac{1}{\Delta x^2 \Delta y^2}\left(\xi_i(x-\Delta x,y,t)+\xi_i(x+\Delta x,y,t) + \xi_i(x,y-\Delta y,t)+\xi_i(x,y+\Delta y,t)-4\xi_i(x,y,t)\right) - \xi_i(x,y,t-\Delta t)\left(\frac{1}{c_0^2\Delta t^2}-\frac{R}{2\rho_0 c_0^2 \Delta t}\right)+\frac{2\xi_i(x,y,t)}{c_0^2\Delta t^2}\right]. \quad (14)$$

The total displacement field vector, as given in (9) is simply the sum of the incident and scattered fields. The next section will discuss boundary conditions as they pertain to the solutions of (13) and (14) in the context of the experimental setup depicted in Fig. (2).

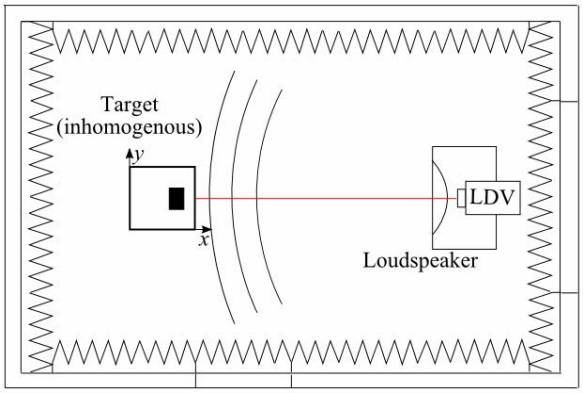

Figure 2. Measurement setup shows collocated LDV and loudspeaker. Plane wave is incident on target surface parallel to *y-z* plane.

Boundary Conditions and Experimental Setup

Fig. 2 depicts the experimental setup used to capture SWEI images of both homogeneous and inhomogeneous targets. A loudspeaker and scanning LDV are positioned at one end of an anechoic chamber. The target is positioned approximately 2.5 m away at the opposite end of the chamber. While distances depicted here are not sufficient for field applications, the maximum standoff capability of the LDV is 30 m and loudspeakers such as a long range acoustic device (LRAD) can easily generate 80-100 dB sound pressure level (SPL) at 1 km.

Imaging of the target's surface is done using a raster scan with each pixel value corresponding to the vibration energy at that point. The excitation used is an LFM chirp from 0.050 – 2.5 kHz with duration of 100 ms. The LDV measures the frequency response of the target at each pixel point, integrating the square of the measured signal in the frequency domain over the bandwidth specified. The energy value measured for each pixel is recorded and the LFM chirp is repeated at the next point.

As depicted in Fig. 2, the farfield distance for the 2.5 kHz stop frequency is 0.24 m, placing the target well into the zone dominated by spherical spreading where wave fronts can be assumed to be planar. For this reason, the boundary conditions for the FDTD simulation of the target's response are

$$\xi(t) = \begin{cases} \dfrac{p_0}{\omega(t) Z_{\text{air}}}\sin(\omega(t)t) & \text{for } x = L_a \\ 0 & \text{for } x = 0,\ y = 0,\ y = L_b \end{cases} \quad (15)$$

where p_0 is the incident sound pressure in Pascals, $\omega(t)$ is the instantaneous frequency, and $Z_{air} = \rho_{\text{air}} c_{\text{air}}$ is the acoustic impedance of air. The zero amplitude boundary condition for left, top, and bottom edges is appropriate for a solid-air boundary where the vast difference in densities results in almost total reflection. As with any FDTD method, stability is ensured by correctly specifying the time step. Each time step must be short enough to allow propagation of the wave's energy from one grid segment to another. Utilizing the velocity equation, a conservative limit for the time step Δt is

$$\Delta t < \frac{1}{3}\frac{\min\left(\left[\Delta x, \Delta y\right]\right)}{c_0}. \quad (16)$$

Results and Discussion

Figs. 3(a) and 3(b) show the simulated results of longitudinal scattering from a 100 ms acoustic LFM chirp. Fig. 3(a) gives the inhomogeneous sound speed, $c_1(\mathbf{x})$, for a 2.5×5×7 cm steel parallelepiped embedded in a 15×23×23 cm block of expanded polystyrene foam, which matches the size and location of the actual test sample shown in Fig. 4. The elasticity, density, and Poisson ratio of the foam is 1 MPa, 10 kgm^{-3} and 0.03 respectively while that of the steel is 200 GPa, 8 kgm^{-3}, and 0.27. Fig. 3(b) shows the energy (sum of the squared time domain samples) resulting from longitudinal scattering in the *x-y* plane. A null in the vibration response is clearly visible adjacent to the inhomogeneity and due to its proximity to the surface, this null can be measured by the LDV as depicted in Fig. 4. The inhomogeneity is affectively creating an acoustic "shadow" as wave energy bounces back and forth within the homogeneous medium. The depth to which inhomogeneities can be detected depends on both its lateral area (parallel to *y-z* plane) and sound amplitude used.

Fig. 4 shows the measured surface response (parallel to the *y-z* plane) for the 2.5×5×7 cm inhomogeneity located at x = 11.75 (2 cm deep), y = 0.12, z = 0.15. The null in vibration energy is clearly visible as the dark blue area directly over the inhomogeneity. Several more experiments were conducted with inhomogeneities farther from the surface with a maximum detection depth of 5 cm for the same 80 dB SPL LFM waveform.

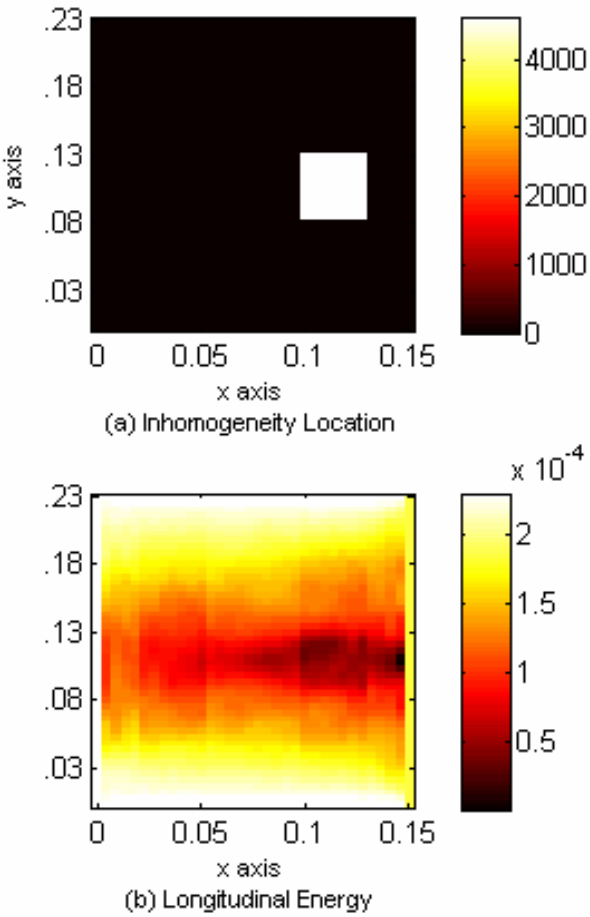

Figure 3. FDTD simulation results: (a) inhomogeneous region sound speed depicts location of 2.5×5×7 cm steel inhomogeneity; and (b) simulation results show weak longitudinal energy at L_a = 0.15 surface due to inhomogeneity.

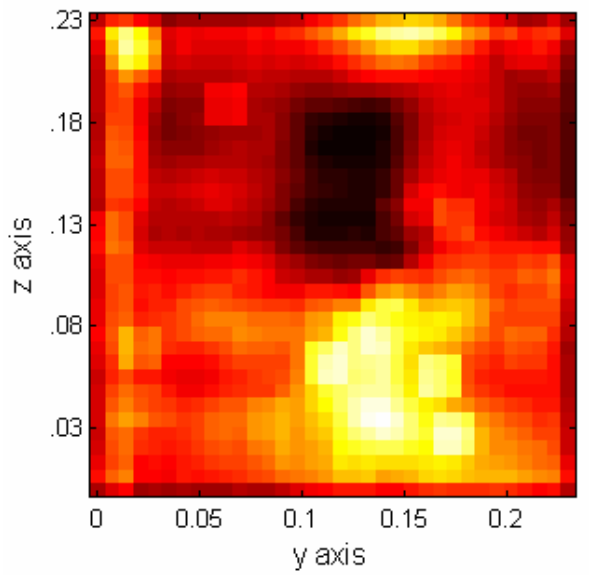

Figure 4. Measurement results show decrease in longitudinal energy caused by 2.5×5×7 cm steel inhomogeneity located at x = 11.75 (2 cm deep), y = 0.12, z = 0.15.

Acknowledgement

This material is based upon work supported by the U.S. Office of Naval Research as a Multi-disciplinary University Research Initiative on Sound and Electromagnetic Interacting Waves under grant number N00014-10-1-0958.

References

1. Gao, L., K. J. Parker, and S. K. Alam, "Sonoelasticity imaging: Theory and experimental verification," Acoustic Society of America Journal, Vol. 97, no. 6, pp. 3875-3886, June 1995.
2. Gennisson, J., S. Catheline, S. Chaffai, and M. Fink, "Transient elastography in anisotropic medium: Application to the measurement of slow and fast shear wave speeds in muscles," Acoustic Society of America Journal, Vol. 114, no. 1, pp. 536-541, July 2003.
3. Parker, K. J., L. Gao, S. K. Alam, D. Rubens, and R. M. Lerner, "Sonoelasticity Imaging: Theory and Application," IEEE Ultrasonics Symposium, pp. 623-628, San Antonio, Texas, Nov. 1996.
4. Xiang, N., and J. M. Sabatier, "An experimental study on antipersonnel landmine detection using acostic-to-seismic coupling," Acoustic Society of America Journal, Vol. 113, no. 3, pp. 1333-1341, Mar. 2003.
5. Xiang, N., and J. M. Sabatier, "Laser Doppler Vibrometer-Based Acoustic Landmine Detection Using the Fast M-Sequence Transform," IEEE Geoscience and Remote Sensing Letters, Vol. 1, no. 4, pp. 292-294, Oct. 2004.
6. Landau, L. D., and E. M. Lifshitz, *Theory of Elasticity*, translated from Russian by J. B. Sykes and W. H. Feid, Pergamon, New York, 1970.